https://doi.org/10.5194/egusphere-2026-6040
Preprint. Discussion started: 19 November 2026
© Author(s) 2026. CC BY 4.0 License.

Color calibrated field photography enables quantitative analysis of ice sheet surface darkening

Shunan Feng[1,2], Beatriz Gill-Olivas[1,2], Emily L. M. Broadwell[1,2], Ravi Sven Peters[3], Helen K. Feord[3], Andreas Westergaard-Nielsen[4], Christopher J. Williamson[5], Nozomu Takeuchi[6], Alexandre Magno Anesio[1,2], Liane G. Benning[3,7], and Martyn Tranter[1,2]

[1]Department of Environmental Science, Aarhus University, Frederiksborgvej 399, DK-4000 Roskilde, Denmark
[2]Arctic Research Cluster, Aarhus University, Denmark
[3]GFZ Helmholtz Centre for Geosciences, Telegrafenberg, 14473 Potsdam, Germany
[4]Department of Geosciences and Natural Resource Management, University of Copenhagen, Øster Voldgade 10, DK-1350 Copenhagen, Denmark
[5]Bristol Glaciology Centre, School of Geographical Sciences,University of Bristol, Bristol, BS8 1SS, United Kingdom
[6]Center for Environmental Remote Sensing, Chiba University, Chiba 263-8522, Japan
[7]Department of Earth Sciences, Freie Universität of Berlin, 12249 Berlin, Germany

Correspondence: Shunan Feng (shunan.feng@envs.au.dk)

Abstract. Glacier and ice sheet surface darkening is driven by various light-absorbing impurities, including glacier ice algae and cryoconite. Quantification of different darkening agents typically requires specialized instrumentation that can be expensive and time-consuming to deploy. We developed a workflow for quantitative darkness analysis of calibrated field photographs. The RAW image processing workflow includes color calibration by a ColorChecker, spatial scale determination, sampling area delineation, and image classification. Calibrated images are converted to the CIELAB color space to derive lightness (L^*). The classifier achieved 93.3% accuracy for cryoconite cover detection when applied to 21 images from a transect on the southwest Greenland Ice Sheet. Glacier ice algal abundance was negatively correlated with surface ice lightness (r^2=0.62, p<0.001), while inclusion of fractional cryoconite cover increased the explained variance by 20% (r^2=0.82, p<0.001). Our workflow helps to make field photography a low cost and user-friendly complementary approach for investigating ice surface darkening.

1 Introduction

The darkening of glacier and ice sheet surfaces is driven by a complex interplay of spatially and temporally variable biophysical processes including snow and ice melt, the accumulation of meltwater, and the abundance of glacier ice algae, mineral dust, and cryoconite material (Tedesco et al., 2015, 2016; Ryan et al., 2018; Cook et al., 2020; Williamson and Tedstone, 2026; Halbach et al., 2025; Feng et al., 2025; Chevrollier et al., 2026). Glacier ice algae, consisting primarily of the genus *Ancylonema*, have emerged as one of the major drivers of ice surface darkening across many glacier and ice sheet ablation zones (Williamson et al., 2020; Halbach et al., 2023). This darkening is achieved due to the heavily pigmented nature of the algal cells (Procházková et al., 2025; Rossel et al., 2025; Feord et al., 2025), initiating a bioalbedo feedback which acts to darken the surface ice (Cook et al., 2017b, a). Whilst direct sampling of surface ice provides valuable groundtruth data on the composition and abundance

https://doi.org/10.5194/egusphere-2026-6040
Preprint. Discussion started: 19 November 2026
© Author(s) 2026. CC BY 4.0 License.

of glacier ice algae and mineral dust (Stibal et al., 2017; Cook et al., 2020; McCutcheon et al., 2021, 2026), field based quantification of glacier ice algal abundance typically requires labor intensive sampling and laboratory analysis. As a result, on site assessment of algal abundance often relies on expert interpretation of surface ice darkness from visual observations and/or field photographs. Similarly, our ability to quantify cryoconite coverage across sites remains limited (Cook et al., 2016; Chevrollier et al., 2026). Cryoconite is a biologically active aggregate of mineral and organic material, bound together by cyanobacteria that acts as a critical darkening agent (Takeuchi, 2002; Cook et al., 2016; Rozwalak et al., 2022). However, the fine grain size of cryoconite granules, often <1 cm in diameter (Rozwalak et al., 2022), makes it difficult to be detected using conventional remote-sensing observations. Furthermore, cryoconite often melts into ice surface to form quasi-circular holes, known as cryoconite holes (Cook et al., 2016; Takeuchi et al., 2018; Feord et al., 2026). Until now, quantification of the collective impacts of glacier ice algae, mineral dust, and cryoconite sediments on ice surface darkness has required specialized instruments, such as albedometers or field spectrometers (Ryan et al., 2017; Cook et al., 2020; Chevrollier et al., 2023), which are expensive to acquire and time-consuming to operate. This has limited the collection of spatially representative groundtruth observations of surface ice darkening across glacial environments, which are often remote and challenging to access.

Close-up field photography, which is routinely undertaken during ice surface sampling campaigns, provides high spatial resolution images that can capture fine scale information on ice surface characteristics, including the surface ice darkness, the distribution of cryoconite sediments (Irvine-Fynn et al., 2010; Rossini et al., 2023) and the development of cryoconite holes (Irvine-Fynn et al., 2011; Takeuchi et al., 2018; Onuma et al., 2018). Despite its widespread use, field photography is typically used only for qualitative interpretation because of differences in camera settings, illumination conditions, and often the lack of ColorChecker. This prohibits the development of image processing workflows to make quantitative comparisons across different sites and studies. Close-up digital photographs acquired in RAW format can be processed while maintaining the linear relationship between digital number and radiance (Akkaynak et al., 2014; Burggraaff et al., 2019), allowing quantitative characterization of surface conditions and has been used for applications such as surface ice classification and land cover mapping (Ryan et al., 2017; Okamoto et al., 2024).

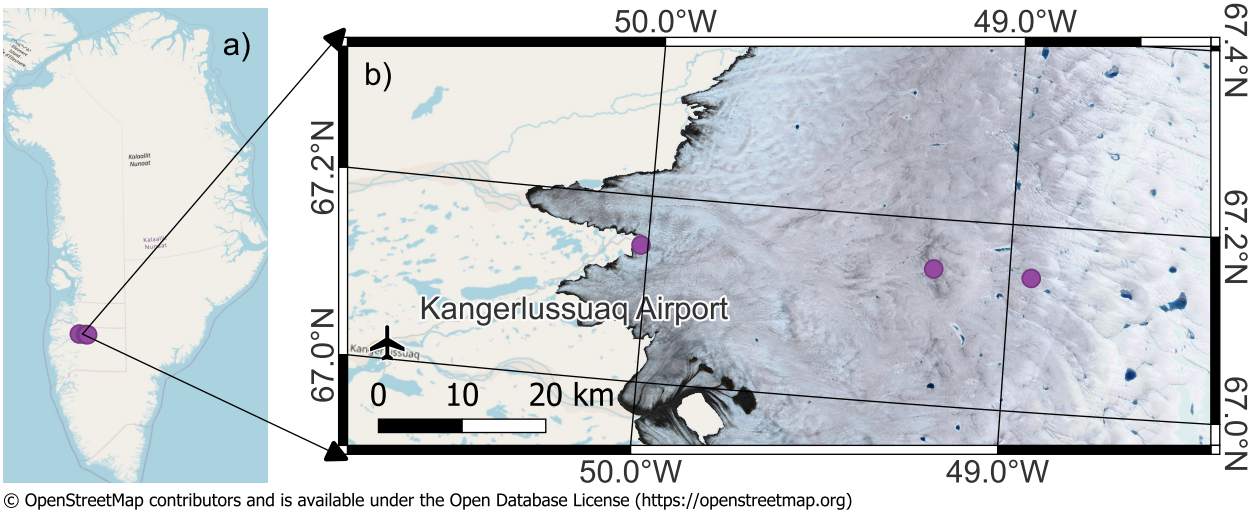
In this study, we developed and tested a workflow for conversion of calibrated field photographs of surface ice into a quantitative surface ice "lightness" (L^*) product. The workflow calibrates RAW images using a ColorChecker reference target and converts the images to the perceptually uniform CIELAB color space (Ohno, 2000; Paschos, 2001; León et al., 2006), from which surface lightness (L^*) can be quantified. Calibration of the images to surface impurities is performed by destructive ice surface sampling, as described below. This allows the us to evaluate the contributions of glacier ice algae and cryoconite (both dispersed cryoconite and cryoconite holes) to the surface ice darkening and establish empirical relationships between L^* described image darkness and measured microbial darkening agents. The image processing workflow is integrated into a cross platform (Windows, macOS, and Linux) desktop software (iCalibrateImages v1.1) that provides a user-friendly interface for image calibration and analysis in various field photography based applications.

https://doi.org/10.5194/egusphere-2026-6040
Preprint. Discussion started: 19 November 2026
© Author(s) 2026. CC BY 4.0 License.

2 Methods

2.1 Field Image Acquisition and Ice Sampling

Close-up images of surface ice and ice surface samples were collected during the 2024 DeepPurple field campaign along a 47 km transect from the ice margin near Kangerlussuaq, Greenland (Fig.1). Field data were collected on 3rd and 4th August 2024 at three sites along the transect from the margin of the ice sheet (Site 1: 67.14677°, -50.01940°) to 47 km inland (Site 2: 67.14642°, -49.20970°; Site 3: 67.14377°, -48.93970°).



© OpenStreetMap contributors and is available under the Open Database License (https://openstreetmap.org)

Figure 1. Sampling sites of the 2024 DeepPurple field campaign along a 47 km transect from the ice margin near Kangerlussuaq, Greenland. The basemap is accessed from © OpenStreetMap contributors and is available under the Open Database License (https://openstreetmap.org). Background satellite imagery is ice optimized harmonized Landsat and Sentinel 2 (Feng et al., 2023) natural color mosaic (2nd-5th August 2024). Non ice areas are masked by the Greenland Ice Sheet Mapping Project (GIMP) ice mask (Howat et al., 2014).

RAW Bayer-pattern color filter array (CFA) images of the ice surface were acquired using a CANON EOS M3 camera and a Calibrite® ColorChecker Classic card adjacent to the sampling point (Fig.2a). The camera was positioned as close to nadir as possible and maintained at a height of ∼1 m above the ice surface. The pixel resolution, i.e., ground sampling distance (GSD), was calculated from the camera settings using Eq.1 (DeWitt and Wolf, 2000; Lisein et al., 2013):

$$\mathrm{GSD} = \frac{H \cdot SW}{f \cdot N} \tag{1}$$

where H is the height above ground, SW is the sensor width, f is the focal length, and N is the image width in pixels. For the CANON EOS M3 (sensor width = 22.3 mm, image width = 6,000 pixels) equipped with an 18 mm lens and positioned 1.0 m above the target, the resulting GSD would be 0.206 mm pixel^{-1}.

https://doi.org/10.5194/egusphere-2026-6040
Preprint. Discussion started: 19 November 2026
© Author(s) 2026. CC BY 4.0 License.

Ice surface samples were subsequently collected from the top 2 cm into sterile Whirl-Pak bags using an ice axe and metal scoop pre-condtioned in supraglacial water. The cellular abundance (cells mL^{-1}) of the algal community was characterized using a 1.8 mL aliquot from the Whirl-Pak bag, fixed with paraformaldehyde (PFA; 2% final concentration). Samples were counted on a FlowCam 5000 (Yokawa Fluid Imaging Technologies, Inc., USA) (Peter et al., 2024; Feord et al., 2025) equipped with a 100 μm $\times$ 700 μm flow cell, a $\times$ 10 objective and using the associated Visual Spreadsheet software (v5.9.0.74, Yokogawa Fluid Imaging Technologies Inc., USA). Each measurement was performed with a flow rate of 0.250 mL min^{-1}, the distance to the nearest neighbor set to 0.1 μm, pixel intensity for both dark and white pixels set to 15, and 5 close hole iterations. The auto image rate was chosen to match the highest possible theoretical efficiency of 71%. Each sample was measured in technical triplicates. Algal cells were subsequently classified as snow algae, unicellular glacier ice algae (*Ancylonema alaskanum*), or filamentous glacier ice algae (*Ancylonema nordenskioldii*) after assessing the morphological characteristics at a magnification at $\times$ 10 objective. For this study, combined abundances of *A. alaskanum* and *A. nordenskioldii* were used. Automated particle classification was complemented by manual inspection (Feord et al., 2025).

2.2 Image Calibration Workflow

RAW Bayer-pattern CFA close-up images (Fig.2a) were processed by following the image calibration pipeline by MathWorks (2026) and Sumner (2014) using the associated image metadata, which included black level, CFA layout, white balance coefficients, and the camera-to-sRGB transform matrix. Raw CFA images were first linearized. After black-level subtraction and white-balance correction, the CFA images were demosaiced to produce true-color images. ColorChecker targets and color patches were automatically detected and identified (Fig.2b) using a deep convolutional neural network (CNN) (Marrero Fernández et al., 2019). It provides automated and repeatable target localization across images with varying ColorChecker positions, scales, illuminations, and viewing angles, while avoiding subjective variation associated with manual selection of all individual color patches. When automatic detection was unsuccessful or incorrect, the four corner fiducial markers of the ColorChecker were manually selected and used as registration points. The ColorChecker detector was used only for ColorChecker identification and registration. The subsequent image calibration was based on the measured ColorChecker patch values and was therefore independent of the CNN model itself. The calibration results are reproducible using either the automated detection workflow or manual ColorChecker selection. No retraining or customization of the ColorChecker detector was performed in this study. Details regarding the CNN architecture, training dataset, model evaluation, and parameter settings are provided by Marrero Fernández et al. (2019).

Color errors for each identified patch were calculated by comparing measured and reference color values. These color errors were subsequently used to derive a color-correction matrix, which was applied to the image to obtain calibrated colors. Spatial scaling was determined from a manually drawn reference line of known length (e.g., the ColorChecker, Fig.2c), allowing calculation of the pixel-to-centimeter ratio and region of interest (ROI) area (cm^2), assuming nadir images. A manually defined polygon ROI (Fig.2d) was used to delineate the sample area by comparing images acquired before and after sampling. The sampled area is visually identifiable from the visible disturbances associated with sampling compared to the surrounding

https://doi.org/10.5194/egusphere-2026-6040
Preprint. Discussion started: 19 November 2026
© Author(s) 2026. CC BY 4.0 License.

undisturbed ice surface. The ROIs were manually digitized around the visibly disturbed surface ice area boundary to ensure consistency between the images and the corresponding cell counts from the ice samples.

To assess the sensitivity of the results to ROI delineation, the original ROI was systematically increased and decreased using buffer distances at 0.5 cm intervals, ranging from -8.5 cm to +8.5 cm. The resulting changes in image-derived surface reflectance metrics were evaluated and are reported in Supplementary Section (Fig. S1-S3).

All processing steps were integrated into a dedicated cross platform (Windows, macOS, and Linux) application, iCalibrateImages v1.1 (Feng, 2026). In total, 27 images were processed and analyzed in the study but only 21 images had corresponding algal cell counts to use in the darkening analysis. Postprocessed images, spatial scale information, and ROI definitions were subsequently exported for image classification and surface darkening analyses.

2.3 Image Classification and Darkening Analysis

CIELAB or L*a*b* color space is a device independent and perceptually uniform color representation system adopted by the Commission Internationale d'Eclairage (CIE) (Ohno, 2000; Paschos, 2001; León et al., 2006). The device independent design allows quantitative cross sensor comparison of colors under variable acquisition conditions. Furthermore, CIELAB was designed to approximate human color perception (Paschos, 2001), which is particularly relevant because targeted sampling of high algal biomass ice is often guided by visual observations (Doting et al., 2022; Jaarsma et al., 2023). Hence, calibrated images stored in sRGB were converted to CIELAB colors using iCalibrateImages for the classification and darkening analysis. The lightness (L*) was used to quantify the surface ice darkness because it is represented independently of chromaticity (a* and b*) (Ohno, 2000; Paschos, 2001; León et al., 2006) and variation in surface brightness can be assessed separately from color information. The average and standard deviation of L* within the ROI were extracted via iCalibrateImages for the darkening analysis.

A random forest classifier (Breiman, 2001) implemented by scikit-learn (Pedregosa et al., 2011) was developed to classify surface ice into cryoconite (both dispersed cryoconite and cryoconite holes) and bare ice. Cryoconite is a biologically active impurity (Ryan et al., 2018), and can be visually similar to aggregates of concentrated glacier ice algae.To improve class separability and reduce the misclassification of glacier ice algae aggregates as cryoconite, the bare ice class was further subdivided into dark ice, representing areas with high glacier ice algal abundance, and white ice, representing the remaining bare ice surface. Training samples consisted of cryoconite granules identified within dispersed cryoconite pixels to avoid the spectral contamination from meltwater within cryoconite holes. A graphical user interface (GUI) based labeling tool (Fig.2e) was developed to facilitate manual training and test sample selection (Nyboe Laursen et al., 2026). In total, 554 reference points were visually identified and labeled as white ice (n=214), dark ice (n=190), and cryoconite (n=150), which were then randomly (random seed = 42) divided into training (n=443) and testing (n=111) datasets while preserving the class proportions. The number of trees (300) was selected to provide a stable ensemble while maintaining practical computational cost. The balanced_subsample weighting feature was turned on because training classes were not represented equally. It also performs well with relatively small manually labeled datasets, requires limited hyperparameter tuning, provides class-probability estimates, and is easier to interpret and reproduce (Brown et al., 2022). Classified pixels with maximum predicted class probability below

https://doi.org/10.5194/egusphere-2026-6040
Preprint. Discussion started: 19 November 2026
© Author(s) 2026. CC BY 4.0 License.

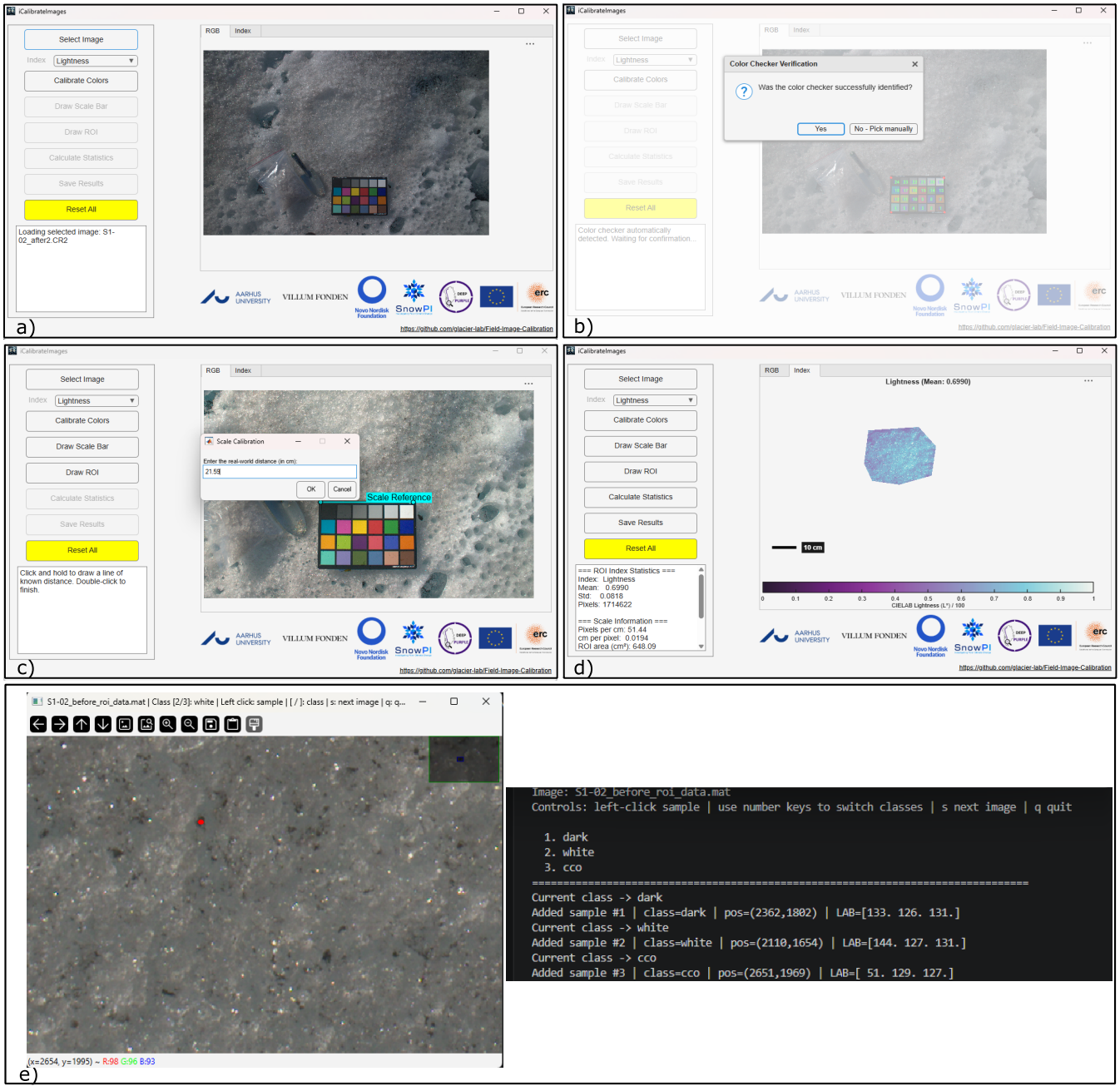


Figure 2. Overview of the image calibration workflow in iCalibrateImages v1.1: (a) RAW image import, (b) automatic ColorChecker and color patch detection, (c) interactive determination of spatial scale and region of interest (ROI), and (d) generation of a lightness (L^*) image and associated zonal statistics. The interface for labeling training data for image classification is also shown (e).

https://doi.org/10.5194/egusphere-2026-6040
Preprint. Discussion started: 19 November 2026
© Author(s) 2026. CC BY 4.0 License.

0.60 were assigned to an additional Unclassified category to avoid forcing low confidence pixels into one of the trained surface classes. The rest of model parameters were using the default settings of scikit-learn (Pedregosa et al., 2011) and all source codes are available in Feng (2026). The classifier was then trained using the training dataset and its performance was evaluated using the testing dataset. Finally, model predictions were combined into two classes, bare ice (white and dark ice) and cryoconite, and applied to classify all pixels within the ROI.

Darkening analysis was conducted first by examining the relationship between glacier ice algae and surface ice lightness (L^*). Natural log-transformed total *Ancylomena* spp. cell concentrations (cells mL^{-1}) were linearly regressed against the corresponding mean L^* values to assess the contribution of glacier ice algae to surface ice darkening. The influence of cryoconite was then evaluated by calculating the fractional cryoconite cover, defined as the area classified as cryoconite divided by the total ROI area. Fractional cryoconite cover and log-transformed *Ancylomena* spp. cell concentrations were subsequently included as predictors in a multiple linear regression model with measured L^* as the response variable.

3 Results and Discussions

3.1 Image Calibration and Classification

High classification accuracy of both bare ice and cryoconite was achieved using the calibrated images when compared to previously labelled classes. Sample images calibrated by iCalibrateImages show the corresponding lightness (L*) values and classifications of bare ice and cryoconite (Fig.3). Fig.3 shows a sample image (Fig.3a) calibrated by iCalibrateImages (Fig.3b), the corresponding lightness (L^*) image (Fig.3c), and the classification of bare ice and cryoconite (Fig.3d). This image calibration allows both the quantitative comparison of surface darkness across sampling sites and subsequent classification of surface cover into bare ice and cryoconite, achieving an accuracy of 93.3% for cryoconite and 79.1% and 81.6% accuracy for white ice and dark ice, respectively, on the independent test dataset (n=111). L^* was the most important predictor, accounting for 72% of the total predictor importance, whereas a^* and b^* both contributed 12%. In total, 21 images were processed, with a median surface lightness (L^*) of 0.69 (median absolute deviation, MAD=0.10; mean±1σ=0.73±0.13), and a median *Ancylomena* spp. cell concentration of 8.240×10^3 (MAD=8.085×10^3 cells mL^{-1}; mean±1σ=$3.921 \times 10^4 \pm 4.220 \times 10^4$ cells mL^{-1}) within median ROI areas of 709 cm^2 (MAD=253 cm^2; mean±1σ=768±347 cm^2). All post-processed images and associated outputs are available at (Feng, 2026).

3.2 Darkening Analysis

Glacier ice algae was a good predictor of L^*, explaining 62% of the observed variability in the test dataset (r^2=0.62, p<0.001, Fig.4a, Eq.2). This result is comparable to previous studies, which reported that glacier ice algae explained 56–60% of the variability in broadband albedo decline with increasing cell concentration (Stibal et al., 2017; Cook et al., 2020).

Close-up RAW images allow us not only to estimate glacier ice algae concentrations but also to identify the presence and spatial distribution of cryoconite. This includes dispersed cryoconite granules within the sampled area. However, glacier ice

https://doi.org/10.5194/egusphere-2026-6040
Preprint. Discussion started: 19 November 2026
© Author(s) 2026. CC BY 4.0 License.

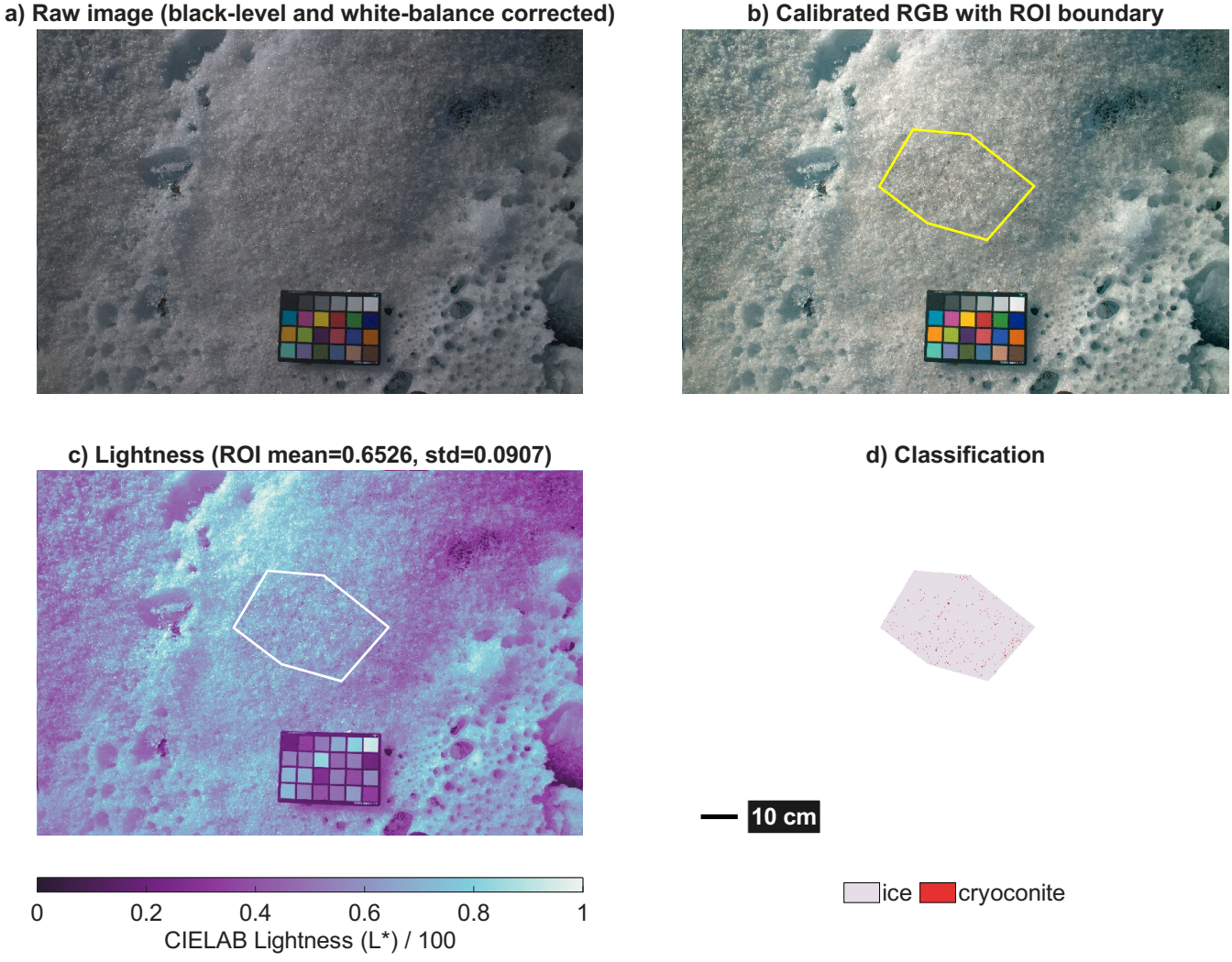


Figure 3. Sample results of image calibration and classification, showing the RAW image after black level and white level correction (a), the ColorChecker calibrated image (b), the corresponding lightness image derived from the CIELAB color space ($L^*/100$) (c), and the classification of ice and cryoconite (d). The region of interest (ROI) is indicated in the RGB and lightness images. Surface ice areas outside the ROI were masked out.

algae can also form small aggregates that are spectrally similar to dispersed cryoconite, and so it is challenging to categorize these as exclusively cryoconite given that the presence of aggregated glacier ice algal cells or other mineral or organic matter cannot be fully discounted without sequencing or *in situ* microscopy. Although cryoconite occupied only a small fraction of the sampled surface ice area on average (2.34% $\pm$ 2.64%), it is an important contributor to surface ice darkening. The combined effects of glacier ice algae and cryoconite on L^* were assessed using a multiple linear regression (MLR) model (Eq.3), with predicted L^* showing strong agreement with the L^* measurements (r^2=0.82, p<0.001, Fig.4), indicating that the combination

https://doi.org/10.5194/egusphere-2026-6040
Preprint. Discussion started: 19 November 2026
© Author(s) 2026. CC BY 4.0 License.

of glacier ice algal abundance (log-transformed cell concentration) and cryoconite fraction explained an additional 20% of the variability in L^* compared with the glacier ice algae alone (Eq.2). Thus, the presented workflow is a highly efficient and effective method for quantifying the coverage of dispersed cryoconite and its impact on surface darkening.

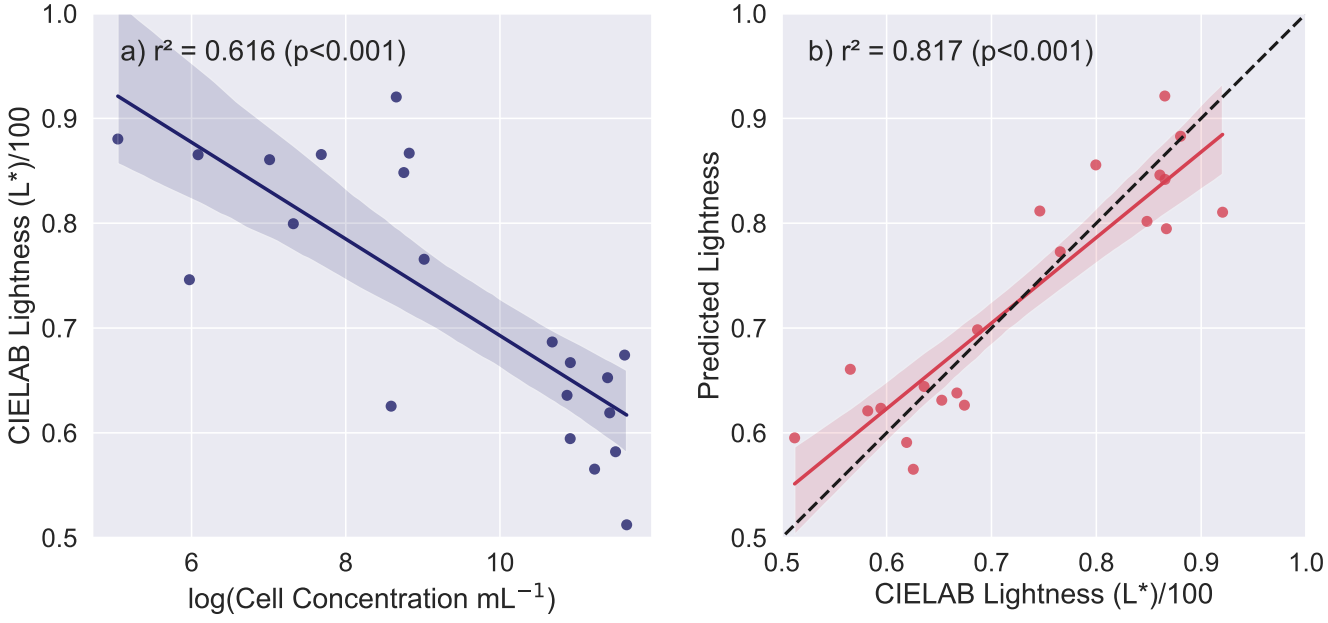


Figure 4. Relationship between average surface ice lightness and cell concentration (log-transformed total *Ancylomena* spp. cell concentration [cells mL^{-1}]; Eq.2) (a), and a multiple linear regression model (Eq.3) predicting surface ice lightness from cell concentration (log-transformed total *Ancylomena* spp. cell concentration [cells mL^{-1}]) and the fraction of cryoconite (b) against actual lightness values. R^2 values ($p < 0.001$) are labeled in the figure. The black dashed line in subfigure b is the 1:1 reference line.

The relationships between glacier ice algal abundance and image lightness, and between glacier ice algal abundance, fractional cryoconite cover, and image lightness, are summarized in Eq.2 and Eq.3, respectively. These empirical relationships demonstrate the potential for estimating glacier ice algal abundance from calibrated field photographs, providing a low-cost, user-friendly, and time-efficient alternative to traditional laboratory analyses.

$$L^* = 1.1536 - 0.0461 \cdot ln(algae) \tag{2}$$

$$L^* = 1.2856 - 0.0547 \cdot ln(algae) - 2.2313 \cdot cryoconite_fraction \tag{3}$$

https://doi.org/10.5194/egusphere-2026-6040
Preprint. Discussion started: 19 November 2026
© Author(s) 2026. CC BY 4.0 License.

3.3 Limitations and Future Work

Various limitations remain in the current processing workflow. The implemented image calibration pipeline does not account for lens distortion, which may restrict the use of some image sensors when lens distortion impact becomes substantial. However, conventional commercial digital cameras are expected to perform well, and the image calibration workflow was successfully tested using a Nikon D7500, Canon EOS R50, Canon EOS M3, and Canon EOS 4000D. Natural ice surfaces are usually not perfectly flat. Therefore, the camera orientation was placed in an approximately nadir position using the judgment of the field operator. In addition, because of the challenging weather conditions and limited time during field sampling on the ice sheet, the camera height of 1 m above the surface ice was estimated manually and may have varied slightly between images. These variations influence the GSD and therefore the physical area of the ROI. However, they do not affect the image calibration workflow because the calibration is based on color correction using the ColorChecker within each image, rather than on the absolute pixel sizes. The pixel size across all processed images is 0.26±0.09 mm, very close to the GSD of 0.25 given a perfect nadir position at 1 m above the ground Eq.1). Hence, we do not expect any substantial impact on the image calibration or the study conclusions given these small variations in viewing geometry and camera height.

Uncertainty associated with manual ROI delineation was evaluated through a sensitivity analysis by systematically increasing and decreasing the ROI by up to 8.5 cm from the original manually defined boundary (Supplementary Section Fig. S1). Changes in mean L^* values were minimal, with differences ranging from 0 to -0.005 relative to the original ROI. The variability increased with increasing buffer distance and the maximum standard deviation reached 0.014. These results indicate that the image derived L^* values are relatively insensitive to reasonable variations in ROI definition and it is unlikely to be a major source of uncertainty in the analysis.

Although digital cameras provide high spatial resolution, their spectral resolution limits the ability to distinguish surface features with similar spectral profiles. Misclassifications occur primarily in sample areas where meltwater has accumulated, as liquid water is an effective darkening agent itself (Greuell, 2000). It is also hard to differentiate between dispersed cryoconite from other biological aggregates and certain mineral particles, since cryoconite is a type of biologically active impurity that contains a mineral fraction (Takeuchi, 2002; Cook et al., 2016; Rozwalak et al., 2022). Therefore, a prior knowledge of the environmental context in which samples were collected will be crucial in assessing the outputs. Samples were collected over a 47-km transect but the sample size was small (n=21). Further sample images were collected, but it was decided that the absence of post-sampling images meant the ROI could not be allocated with the specificity needed for quantitative analysis. The empirical relationships described in Eq. 2 and 3, derived from the transect on the Greenland Ice Sheet, therefore require validation at additional sites. Finally, image lightness cannot be directly translated into broadband albedo, which requires characterization of sensor spectral sensitivity and radiometric calibration using reference reflectance targets (Ryan et al., 2017), such as a Spectralon panel.

Future developments will focus on expanding the collection of *in situ* data to improve and validate the empirical prediction models (Eq.2 and 3) via large collaborative fieldwork campaigns such as Cryospheric Algal Sampling Protocols (CASP-ICE). The imaging system can also be integrated into automatic weather stations to provide continuous monitoring of surface ice

https://doi.org/10.5194/egusphere-2026-6040
Preprint. Discussion started: 19 November 2026
© Author(s) 2026. CC BY 4.0 License.

darkening. We also aim to improve classification approaches and develop radiometric calibration procedures and desktop applications to enable direct estimation of surface albedo from field photographs.

4 Conclusions

We present iCalibrateImages v1.1, a desktop application that integrates a RAW image processing pipeline, including image calibration with a ColorChecker, spatial scale determination, ROI delineation, and image classification for quantitative analysis of surface ice darkening. By converting calibrated images to the CIELAB color space, surface ice lightness (L*) can be quantified and linked to biological and particulate impurities responsible for ice darkening.

Glacier ice algal concentration proves to be a good predictor of lightness (r^2=0.62), while the inclusion of fractional cryoconite cover in a multiple linear regression model increased the explained variance to 82%. These results are consistent with previous studies demonstrating the importance of glacier ice algae as a primary driver of surface darkening and further highlight the important contribution of cryoconite. The ability to identify and quantify both dispersed cryoconite and cryoconite holes from calibrated close-range imagery provides a practical advantage over traditional qualitative field observations.

Overall, calibrated field photography is a low-cost, user-friendly, and time-efficient approach for investigating surface ice darkening. The approach allows quantitative cross site comparison and is useful for generating rapid first-order estimates of glacier ice algal abundance and fractional cryoconite cover. Further work is needed to improve classification accuracy, radiometric calibration, and model transferability across sites and imaging systems, yet the workflow demonstrates considerable potential for providing complementary data for glacier monitoring and future studies of bioalbedo darkening processes.

Code and data availability. All source code, the desktop application iCalibrateImages v1.1 (available for Windows, macOS, and Linux with the support of MATLAB app designer), postprocessed images, and cell counts are all available on Zenodo (Feng, 2026). Future software development, updates, and links to associated supporting materials will be released through the corresponding GitHub repository: https://github.com/glacier-lab/Field-Image-Calibration.

Author contributions. Conceptualization: SF, BGO, AWN. Data curation: SF, BGO, ELMB, RSP, HkF. Formal analysis: SF, BGO, ELMB. Funding acquisition: SF, AWN, AMA, LGB, MT. Investigation: SF, BGO, ELMB. Methodology: SF, BGO, AWN. Project administration: AMA, LGB, MT. Resources: SF, BGO, ELMB, RSP. Software: SF. Supervision: AWN, AMA, LGB, MT. Validation: SF, BGO, ELMB. Visualization: SF. Writing – original draft: SF, BGO, ELMB. Writing – review & editing: all coauthors.

Competing interests. The authors declare that they have no conflict of interest.

https://doi.org/10.5194/egusphere-2026-6040
Preprint. Discussion started: 19 November 2026
© Author(s) 2026. CC BY 4.0 License.



Acknowledgements. This publication is supported by the Novo Nordisk Foundation (grant No. NNF24OC0094957) and the Villum foundation (project No. 42069 and No. 69596). It is also part of the Deep Purple Project, funded by the European Research Council (ERC) under the European Union's Horizon 2020 research and innovation program (grant agreement No. 856416), and the SnowPI project, funded by the European Union's Horizon Europe Research and Innovation Program under Grant Agreement No. 101184939. Views and opinions expressed are however those of the author(s) only and do not necessarily reflect those of the European Union or the European Climate, Infrastructure and Environment Executive Agency (CINEA). Neither the European Union nor CINEA can be held responsible for them. Additional funding is provided by JSPS KAKENHI 25K22868 & 24H00260, the National Environmental Research Council of the UK "CASP-ICE" award (NE/Y002636/1), and the Helmholtz Recruiting Initiative (grant no. I-044-16-01). We also thank Rasmus Henrik Amund Henriksen, Lucas Horstmann, Erkin Gözdereliler, and Ben Johnson for their assistance in testing the software.

We sincerely thank the editor Prof. Richard Kelly for his constructive and detailed feedback, and the support throughout the review process.

https://doi.org/10.5194/egusphere-2026-6040
Preprint. Discussion started: 19 November 2026
© Author(s) 2026. CC BY 4.0 License.

References

Akkaynak, D., Treibitz, T., Xiao, B., Gürkan, U. A., Allen, J. J., Demirci, U., and Hanlon, R. T.: Use of commercial off-the-shelf digital cameras for scientific data acquisition and scene-specific color calibration, Journal of the Optical Society of America A, 31, 312, https://doi.org/10.1364/JOSAA.31.000312, 2014.

Breiman, L.: Random Forests, Machine Learning 2001 45:1, 45, 5–32, https://doi.org/10.1023/A:1010933404324, 2001.

Brown, C. F., Brumby, S. P., Guzder-Williams, B., Birch, T., Hyde, S. B., Mazzariello, J., Czerwinski, W., Pasquarella, V. J., Haertel, R., Ilyushchenko, S., Schwehr, K., Weisse, M., Stolle, F., Hanson, C., Guinan, O., Moore, R., and Tait, A. M.: Dynamic World, Near real-time global 10 m land use land cover mapping, Scientific Data, 9, 251, https://doi.org/10.1038/s41597-022-01307-4, 2022.

Burggraaff, O., Schmidt, N., Zamorano, J., Pauly, K., Pascual, S., Tapia, C., Spyrakos, E., and Snik, F.: Standardized spectral and radiometric calibration of consumer cameras, Optics Express, 27, 19 075, https://doi.org/10.1364/OE.27.019075, 2019.

Chevrollier, L.-A., Cook, J. M., Halbach, L., Jakobsen, H., Benning, L. G., Anesio, A. M., and Tranter, M.: Light absorption and albedo reduction by pigmented microalgae on snow and ice, Journal of Glaciology, 69, 333–341, https://doi.org/10.1017/jog.2022.64, 2023.

Chevrollier, L.-A., Wehrlé, A., Cook, J. M., Blukis, R., Stevens, I. T., Benning, L. G., Anesio, A. M., and Tranter, M.: Surface processes darkening the southwestern ice sheet of Kalaallit Nunaat (Greenland), Science Advances, 12, eady9482, https://doi.org/10.1126/sciadv.ady9482, 2026.

Cook, J., Edwards, A., Takeuchi, N., and Irvine-Fynn, T.: Cryoconite: The dark biological secret of the cryosphere, Progress in Physical Geography: Earth and Environment, 40, 66–111, https://doi.org/10.1177/0309133315616574, 2016.

Cook, J. M., Hodson, A. J., Gardner, A. S., Flanner, M., Tedstone, A. J., Williamson, C., Irvine-Fynn, T. D. L., Nilsson, J., Bryant, R., and Tranter, M.: Quantifying bioalbedo: a new physically based model and discussion of empirical methods for characterising biological influence on ice and snow albedo, The Cryosphere, 11, 2611–2632, https://doi.org/10.5194/tc-11-2611-2017, 2017a.

Cook, J. M., Hodson, A. J., Taggart, A. J., Mernild, S. H., and Tranter, M.: A predictive model for the spectral "bioalbedo" of snow, Journal of Geophysical Research: Earth Surface, 122, 434–454, https://doi.org/10.1002/2016JF003932, 2017b.

Cook, J. M., Tedstone, A. J., Williamson, C., McCutcheon, J., Hodson, A. J., Dayal, A., Skiles, M., Hofer, S., Bryant, R., McAree, O., McGonigle, A., Ryan, J., Anesio, A. M., Irvine-Fynn, T. D. L., Hubbard, A., Hanna, E., Flanner, M., Mayanna, S., Benning, L. G., van As, D., Yallop, M., McQuaid, J. B., Gribbin, T., and Tranter, M.: Glacier algae accelerate melt rates on the south-western Greenland Ice Sheet, The Cryosphere, 14, 309–330, https://doi.org/10.5194/tc-14-309-2020, 2020.

DeWitt, B. A. and Wolf, P. R.: Elements of Photogrammetry(with Applications in GIS), McGraw-Hill Higher Education, 3rd edn., ISBN 0072924543, 2000.

Doting, E. L., Davie-Martin, C. L., Johansen, A., Benning, L. G., Tranter, M., Rinnan, R., and Anesio, A. M.: Greenland Ice Sheet Surfaces Colonized by Microbial Communities Emit Volatile Organic Compounds, Frontiers in Microbiology, 13, 1–14, https://doi.org/10.3389/fmicb.2022.886293, 2022.

Feng, S.: glacier-lab/Field-Image-Calibration: iCalibrateImages , https://doi.org/10.5281/zenodo.21742413, 2026.

Feng, S., Cook, J. M., Anesio, A. M., Benning, L. G., and Tranter, M.: Long time series (1984–2020) of albedo variations on the Greenland ice sheet from harmonized Landsat and Sentinel 2 imagery, Journal of Glaciology, 69, 1225–1240, https://doi.org/10.1017/jog.2023.11, 2023.

Feng, S., Williamson, C. J., Cook, J. M., Onuma, Y., Takeuchi, N., Magno Anesio, A., Benning, L. G., and Tranter, M.: A new dark ice albedo threshold and its applications, Environmental Research Letters, 20, 084 066, https://doi.org/10.1088/1748-9326/adeea9, 2025.

https://doi.org/10.5194/egusphere-2026-6040
Preprint. Discussion started: 19 November 2026
© Author(s) 2026. CC BY 4.0 License.

Feord, H. K., Trautwein-Schult, A., Keuschnig, C., Ostrzinski, A., Peter, E. K., Jaeger, C., Lisec, J., Mourot, R., Peters, R. S., Çiftçi, O., Tranter, M., Anesio, A. M., Becher, D., and Benning, L. G.: Algae-dominated metaproteomes uncover cellular adaptations to life on the Greenland Ice Sheet, npj Biofilms and Microbiomes, 11, 181, https://doi.org/10.1038/s41522-025-00770-2, 2025.

Feord, H. K., Zervas, A., Sipes, K., Jaarsma, A. H., Tranter, M., Benning, L. G., and Anesio, A. M.: Highly stable active core microbiomes in Greenland cryoconite holes during the bare ice period, FEMS Microbiology Ecology, 102, 74, https://doi.org/10.1093/femsec/fiag074, 2026.

Greuell, W.: Melt–water accumulation on the surface of the greenland ice sheet: effect on albedo and mass balance, Geografiska Annaler: Series A, Physical Geography, 82, 489–498, https://doi.org/10.1111/j.0435-3676.2000.00136.x, 2000.

Halbach, L., Chevrollier, L.-A., Cook, J. M., Stevens, I. T., Hansen, M., Anesio, A. M., Benning, L. G., and Tranter, M.: Dark ice in a warming world: advances and challenges in the study of Greenland Ice Sheet's biological darkening, Annals of Glaciology, pp. 1–6, https://doi.org/10.1017/aog.2023.17, 2023.

Halbach, L., Kitzinger, K., Hansen, M., Littmann, S., Benning, L. G., Bradley, J. A., Whitehouse, M. J., Olofsson, M., Mourot, R., Tranter, M., Kuypers, M. M. M., Ellegaard-Jensen, L., and Anesio, A. M.: Single-cell imaging reveals efficient nutrient uptake and growth of microalgae darkening the Greenland Ice Sheet, Nature Communications 2025 16:1, 16, 1–14, https://doi.org/10.1038/s41467-025-56664-6, 2025.

Howat, I. M., Negrete, A., and Smith, B. E.: The Greenland Ice Mapping Project (GIMP) land classification and surface elevation data sets, The Cryosphere, 8, 1509–1518, https://doi.org/10.5194/tc-8-1509-2014, 2014.

Irvine-Fynn, T. D., Bridge, J. W., and Hodson, A. J.: Rapid quantification of cryoconite: granule geometry and in situ supraglacial extents, using examples from Svalbard and Greenland, Journal of Glaciology, 56, 297–308, https://doi.org/10.3189/002214310791968421, 2010.

Irvine-Fynn, T. D., Bridge, J. W., and Hodson, A. J.: In situ quantification of supraglacial cryoconite morphodynamics using time-lapse imaging: an example from Svalbard, Journal of Glaciology, 57, 651–657, https://doi.org/10.3189/002214311797409695, 2011.

Jaarsma, A. H., Sipes, K., Zervas, A., Jiménez, F. C., Ellegaard-Jensen, L., Thøgersen, M. S., Stougaard, P., Benning, L. G., Tranter, M., and Anesio, A. M.: Exploring microbial diversity in Greenland Ice Sheet supraglacial habitats through culturing-dependent and -independent approaches, FEMS Microbiology Ecology, 99, 1–16, https://doi.org/10.1093/femsec/fiad119, 2023.

León, K., Mery, D., Pedreschi, F., and León, J.: Color measurement in L*a*b* units from RGB digital images, Food Research International, 39, 1084–1091, https://doi.org/10.1016/j.foodres.2006.03.006, 2006.

Lisein, J., Linchant, J., Lejeune, P., Bouché, P., and Vermeulen, C.: Aerial Surveys Using an Unmanned Aerial System (UAS): Comparison of Different Methods for Estimating the Surface Area of Sampling Strips, Tropical Conservation Science, 6, 506–520, https://doi.org/10.1177/194008291300600405, 2013.

Marrero Fernández, P. D., Guerrero Peña, F. A., Ing Ren, T., and Leandro, J. J.: Fast and robust multiple ColorChecker detection using deep convolutional neural networks, Image and Vision Computing, 81, 15–24, https://doi.org/10.1016/j.imavis.2018.11.001, 2019.

MathWorks: Implement Digital Camera Processing Pipeline - MATLAB & Simulink, https://se.mathworks.com/help/images/end-to-end-implementation-of-digital-camera-processing-pipeline.html, 2026.

McCutcheon, J., Lutz, S., Williamson, C., Cook, J. M., Tedstone, A. J., Vanderstraeten, A., Wilson, S. A., Stockdale, A., Bonneville, S., Anesio, A. M., Yallop, M. L., McQuaid, J. B., Tranter, M., and Benning, L. G.: Mineral phosphorus drives glacier algal blooms on the Greenland Ice Sheet, Nature Communications, 12, 570, https://doi.org/10.1038/s41467-020-20627-w, 2021.

https://doi.org/10.5194/egusphere-2026-6040
Preprint. Discussion started: 19 November 2026
© Author(s) 2026. CC BY 4.0 License.

McCutcheon, J., McQuaid, J. B., Canha, N., Barr, S. L., Lutz, S., Roddatis, V., Mayanna, S., Tedstone, A. J., Tranter, M., and Benning, L. G.: Atmospheric Deposition of Local Mineral Dust Delivers Phosphorus to the Greenland Ice Sheet, Environmental Science & Technology, 60, 2515–2527, https://doi.org/10.1021/acs.est.5c13873, 2026.

Nyboe Laursen, S., Feng, S., Smart, A., Grillini, F., Rieksta, J., Jiao, Y., Davie-Martin, C. L., Seco, R., Rinnan, R., and Westergaard-Nielsen, A.: Reduced BVOC emissions from birch forest understory during coupled insect outbreak and microclimatic forcing, Communications Earth & Environment, https://doi.org/10.1038/s43247-026-04057-y, 2026.

Ohno, Y.: CIE Fundamentals for Color Measurements, NIP & Digital Fabrication Conference, 16, 540–545, https://doi.org/10.2352/ISSN.2169-4451.2000.16.1.art00033_2, 2000.

Okamoto, R., Ide, R., and Oguma, H.: Automatically drawing vegetation classification maps using digital time-lapse cameras in alpine ecosystems, Remote Sensing in Ecology and Conservation, 10, 188–202, https://doi.org/10.1002/rse2.364, 2024.

Onuma, Y., Takeuchi, N., Tanaka, S., Nagatsuka, N., Niwano, M., and Aoki, T.: Observations and modelling of algal growth on a snowpack in north-western Greenland, Cryosphere, 12, 2147–2158, https://doi.org/10.5194/tc-12-2147-2018, 2018.

Paschos, G.: Perceptually uniform color spaces for color texture analysis: an empirical evaluation, IEEE Transactions on Image Processing, 10, 932–937, https://doi.org/10.1109/83.923289, 2001.

Pedregosa, F., Varoquaux, G., Gramfort, A., Michel V. and Thirion, B., Grisel, O., Blondel, M., Prettenhofer P. and Weiss, R., Dubourg, V., Vanderplas, J., Passos, A., Cournapeau, D., Brucher, M., Perrot, M., and Duchesnay, E.: Scikit-learn: Machine Learning in Python, Journal of Machine Learning Research, 12, 2825–2830, 2011.

Peter, E. K., Jaeger, C., Lisec, J., Peters, R. S., Mourot, R., Rossel, P. E., Tranter, M., Anesio, A. M., and Benning, L. G.: Endometabolic profiling of pigmented glacier ice algae: the impact of sample processing, Metabolomics, 20, 98, https://doi.org/10.1007/s11306-024-02147-6, 2024.

Procházková, L., Mojzeš, P., Ráček, J., Nedbalová, L., and Remias, D.: Phenolic Iron Complexes Protect Glacier Ice Algae (Zygnematophyceae) Against Excessive <scp>UV</scp> and <scp>VIS</scp> Irradiation, Environmental Microbiology Reports, 17, e70 149, https://doi.org/10.1111/1758-2229.70149, 2025.

Rossel, P. E., Antony, R., Mourot, R., Dittmar, T., Anesio, A. M., Tranter, M., and Benning, L. G.: Dynamics of organic matter in algal blooms on the Greenland ice sheet, Scientific Reports 2025 15:1, 15, 1–12, https://doi.org/10.1038/s41598-025-92182-7, 2025.

Rossini, M., Garzonio, R., Panigada, C., Tagliabue, G., Bramati, G., Vezzoli, G., Cogliati, S., Colombo, R., and Di Mauro, B.: Mapping Surface Features of an Alpine Glacier through Multispectral and Thermal Drone Surveys, Remote Sensing, 15, 3429, https://doi.org/10.3390/rs15133429, 2023.

Rozwalak, P., Podkowa, P., Buda, J., Niedzielski, P., Kawecki, S., Ambrosini, R., Azzoni, R. S., Baccolo, G., Ceballos, J. L., Cook, J., Di Mauro, B., Ficetola, G. F., Franzetti, A., Ignatiuk, D., Klimaszyk, P., Łokas, E., Ono, M., Parnikoza, I., Pietryka, M., Pittino, F., Poniecka, E., Porazinska, D. L., Richter, D., Schmidt, S. K., Sommers, P., Souza-Kasprzyk, J., Stibal, M., Szczuciński, W., Uetake, J., Wejnerowski, b., Yde, J. C., Takeuchi, N., and Zawierucha, K.: Cryoconite – From minerals and organic matter to bioengineered sediments on glacier's surfaces, Science of The Total Environment, 807, 150 874, https://doi.org/10.1016/j.scitotenv.2021.150874, 2022.

Ryan, J. C., Hubbard, A., Box, J. E., Brough, S., Cameron, K., Cook, J. M., Cooper, M., Doyle, S. H., Edwards, A., Holt, T., Irvine-Fynn, T., Jones, C., Pitcher, L. H., Rennermalm, A. K., Smith, L. C., Stibal, M., and Snooke, N.: Derivation of High Spatial Resolution Albedo from UAV Digital Imagery: Application over the Greenland Ice Sheet, Frontiers in Earth Science, 5, https://doi.org/10.3389/feart.2017.00040, 2017.

https://doi.org/10.5194/egusphere-2026-6040
Preprint. Discussion started: 19 November 2026
© Author(s) 2026. CC BY 4.0 License.



Ryan, J. C., Hubbard, A., Stibal, M., Irvine-Fynn, T. D., Cook, J., Smith, L. C., Cameron, K., and Box, J.: Dark zone of the Greenland Ice Sheet controlled by distributed biologically-active impurities, Nature Communications, 9, 1065, https://doi.org/10.1038/s41467-018-03353-2, 2018.

Stibal, M., Box, J. E., Cameron, K. A., Langen, P. L., Yallop, M. L., Mottram, R. H., Khan, A. L., Molotch, N. P., Chrismas, N. A. M., Calì Quaglia, F., Remias, D., Smeets, C. J. P. P., Broeke, M. R., Ryan, J. C., Hubbard, A., Tranter, M., As, D., and Ahlstrøm, A. P.: Algae Drive Enhanced Darkening of Bare Ice on the Greenland Ice Sheet, Geophysical Research Letters, 44, 11,463–11,471, https://doi.org/10.1002/2017GL075958, 2017.

Sumner, R.: Processing RAW Images in MATLAB, Tech. rep., University of California, Santa Cruz, https://rcsumner.net/raw{_}guide/RAWguide.pdf, 2014.

Takeuchi, N.: Optical characteristics of cryoconite (surface dust) on glaciers: The relationships between light absorbency and the property of organic matter contained in the cryoconite, Annals of Glaciology, 34, 409–414, https://doi.org/10.3189/172756402781817743, 2002.

Takeuchi, N., Sakaki, R., Uetake, J., Nagatsuka, N., Shimada, R., Niwano, M., and Aoki, T.: Temporal variations of cryoconite holes and cryoconite coverage on the ablation ice surface of Qaanaaq Glacier in northwest Greenland, Annals of Glaciology, 59, 21–30, https://doi.org/10.1017/aog.2018.19, 2018.

Tedesco, M., Doherty, S., Warren, S., Tranter, M., Stroeve, J. C., Fettweis, X., and Alexander, P.: What Darkens the Greenland Ice Sheet?, Eos, 96, 5–7, https://doi.org/10.1029/2015EO035773, 2015.

Tedesco, M., Doherty, S., Fettweis, X., Alexander, P., Jeyaratnam, J., and Stroeve, J. C.: The darkening of the Greenland ice sheet: trends, drivers, and projections (1981–2100), The Cryosphere, 10, 477–496, https://doi.org/10.5194/tc-10-477-2016, 2016.

Williamson, C. J. and Tedstone, A. J.: Ubiquitous and expanding glacier algal blooms modelled around the Greenland Ice Sheet, Communications Earth & Environment 2026, https://doi.org/10.1038/S43247-026-03758-8, 2026.

Williamson, C. J., Cook, J., Tedstone, A., Yallop, M., McCutcheon, J., Poniecka, E., Campbell, D., Irvine-Fynn, T., McQuaid, J., Tranter, M., Perkins, R., and Anesio, A.: Algal photophysiology drives darkening and melt of the Greenland Ice Sheet, Proceedings of the National Academy of Sciences, 117, 5694–5705, https://doi.org/10.1073/pnas.1918412117, 2020.